J. Luis Deán, Cristina Trillo, Ángel F. Doval and José L. Fernández, "Full-field localization of plate-thickness inhomogeneities through the local changes in the wavenumber of Lamb waves measured with pulsed TV holography," Proc. SPIE 7098, "Eighth International Conference on Vibration Measurements by Laser Techniques: Advances and Applications", 70980F (June 17, 2008)

http://dx.doi.org/10.1117/12.802983

Full-field localization of plate-thickness inhomogeneities through the local changes in the wavenumber of Lamb waves measured with pulsed TV holography

J. Luis Deán, Cristina Trillo, Ángel F. Doval* and José L. Fernández

Universidad de Vigo. Departamento de Física Aplicada. E.T.S. de Ingenieros Industriales. Campus de Lagoas-Marcosende. E36310 Vigo, Spain.

ABSTRACT

A new capability of TV holography, also known as electronic speckle pattern interferometry (ESPI), is presented for locating and imaging slightly thinned or thickened areas in metallic plates. It is based on the measurement of the wavenumber variation of narrowband Lamb waves as they propagate through these plate-thickness inhomogeneities. The relation between frequency and phase velocity of all Lamb modes depends on the elastic constants of the material the plate is made of (two parameters in isotropic materials) and on the plate thickness. Therefore, the associated dispersion curve of each mode present wavenumber changes that are sensitive to a thickness reduction. We have formerly developed a double-pulsed TV holography system which allows the full-field measurement of the instantaneous out-of-plane displacement field induced by surface acoustic waves and, by further processing, to calculate maps of the acoustic amplitude and phase. A method based on further analysis of the acoustic complex-displacement map is therefore proposed to locate and characterize such smooth thickness reductions. In particular, we calculate a map of the local wavenumber of the acoustic wave as the modulus of the two-dimensional gradient of the mechanical phase. Hence, as the variations in the wavenumber correspond to variations in the plate thickness, the local thickness reductions and increments can be detected in this map. Within the resolution limits imposed by the wavelength of the Lamb wave, this method allows also to contour the shape of the inhomogeneities. The technique is demonstrated herein by imaging a X-shaped recess machined on an aluminium plate.

Keywords: ESPI, TV holography, Lamb waves, non-destructive testing

1. INTRODUCTION

Lamb waves are a well-known kind of acoustic waves which originate in stress-free plates as a consequence of the superposition of longitudinal and shear waves successively reflected in the plate faces. They have been widely used for the non-destructive testing of plate materials, presenting many advantages over the traditional C-scanning techniques with bulk waves.[1]

Extensive use has been made of Lamb waves for the location of flaws in plates, and many techniques have been reported on the subject. Usually, the defect detection is based on the measurement of the wavefronts originated in the damaged area, since strong changes of thickness produce wave phenomena such as reflection, scattering or mode conversion which are easily noticeable as changes of the amplitude or phase of the surface displacement field. Then, it is possible to locate flaws like notches[2,3] or cylinder-shaped defects.[4]

The characterization of a plate with Lamb waves can also be conducted so that, provided that the elastic constants of the plate material are known, the plate thickness can be measured since the phase and/or group velocities of a given Lamb mode at a certain frequency depend on this parameter.[5] Subtle thickness variations very seldom affect the shape of the original wavefront enough to be directly detected; in most cases they just induce a local variation of some features of the wave, so the detection of a thinned or thickened area can be approached by measuring smooth changes in any of these features.[6,7]

All the techniques cited above are based on the recording of the temporal evolution of the displacement of several points of the plate surface by means of pointwise techniques. A different approach to detect the

*A.F.D.: E-mail: adoval@uvigo.es

Eighth International Conference on Vibration Measurements by Laser Techniques: Advances and Applications, edited by Enrico Primo Tomasini, Proc. of SPIE Vol. 7098, 70980F, (2008) 0277-786X/08/$18 doi: 10.1117/12.802983

waves consists in obtaining the 2D displacements map of the plate surface by means of a full-field interferometric technique like TV holography (TVH). In fact, TVH has been successfully used to visualize the wavefront distortion by small localized defects[8] or, by numerically solving the inverse scattering problem, to image the shape of larger flaws.[9]

In this communication, we propose and demonstrate a new approach consisting in the use of maps of the Lamb wavenumber to image thickness inhomogeneities in thin plates. Each of these maps will be calculated from a single full-field measurement of the instant displacement of the surface induced by the wave, obtained with pulsed TV holography. Therefore, transient Lamb waves can be used and measured before they reach the edges of the specimen thus avoiding the need for acoustic absorbers to prevent reflections and the subsequent formation of standing waves.

The most relevant aspects of the underlying theory supporting this technique are summarised in section 2, the characteristics of the experimental set-up are described in sections 3.1, 3.2 and 3.3. The technique used to measure the complex representation of the instant displacement of the surface, that we have already presented elsewhere, is succinctly sketched in section 3.3 and the details of the implementation of the wavenumber mapping process are detailed in section 3.4. Finally, some experimental results demonstrating the viability of the proposed inspection method are shown in section 4.

2. THEORY

2.1 Dependence of the wavenumber with the plate thickness for Lamb waves

The dispersive nature of Lamb waves is well known. They are guided acoustic waves in thin plates and show multiple propagation modes. These modes are categorised either as symmetric —denoted S0, S1, ..., Si, ...— or antisymmetric —denoted A0, A1, ..., Ai, ...— according to the symmetry of the displacement associated to the wave with respect to the mean plane of the plate.

The wave parameters, frequency f and wavenumber k, of Lamb waves propagating in a given plate or slab are connected with the velocities of longitudinal c_{L} and shear c_{T} waves in the same material as well as with the thickness $2h$ of the plate through the complex-valued equation[10]

$$F^{\,\mathrm{S}}_{\mathrm{A}} = \frac{\tan\frac{\pi}{2}\sqrt{\gamma^2\chi^2-\xi^2}}{\tan\frac{\pi}{2}\sqrt{\gamma^2-\xi^2}} + \left[\frac{4\xi^2\sqrt{\gamma^2\chi^2-\xi^2}\sqrt{\gamma^2-\xi^2}}{(2\xi^2-\gamma^2\chi^2)^2}\right]^{\pm 1} = 0 \tag{1}$$

which is written in dimensionless form by taking

$$\xi = \frac{2h}{\pi}k \quad \text{, the normalized wavenumber,} \tag{2}$$

$$\gamma = \frac{2h}{\pi c_{\mathrm{L}}}\omega = \frac{4h}{c_{\mathrm{L}}}f \quad \text{, the normalized frequency, and} \tag{3}$$

$$\chi = \frac{c_{\mathrm{L}}}{c_{\mathrm{T}}} \quad \text{, the velocity ratio.} \tag{4}$$

The velocities c_{L} and c_{T} and, consequently, their ratio χ are characteristics of the material the plate is made of. Once the material has been chosen, two sets of real values of γ that satisfy Equation 1 with the $+1$ and -1 exponents can be calculated for each real value of ξ. The resulting families of curves

$$\gamma_{\mathrm{S}i} = \gamma_{\mathrm{S}i}(\xi) \tag{5a}$$

$$\gamma_{\mathrm{A}i} = \gamma_{\mathrm{A}i}(\xi) \tag{5b}$$

are known as the frequency spectra of the symmetric and antisymmetric modes, respectively, of the Lamb waves that can propagate on the plate. The frequency spectrum of Lamb waves is usually represented following Equations 5a and 5b, which are obtained numerically, as shown in Figure 1a.

Since the normalized frequency γ is proportional to the thickness of the plate $2h$ (Equation 3) when a Lamb wave propagates into a region of the plate with a different thickness $2h'$ its normalized frequency changes, though

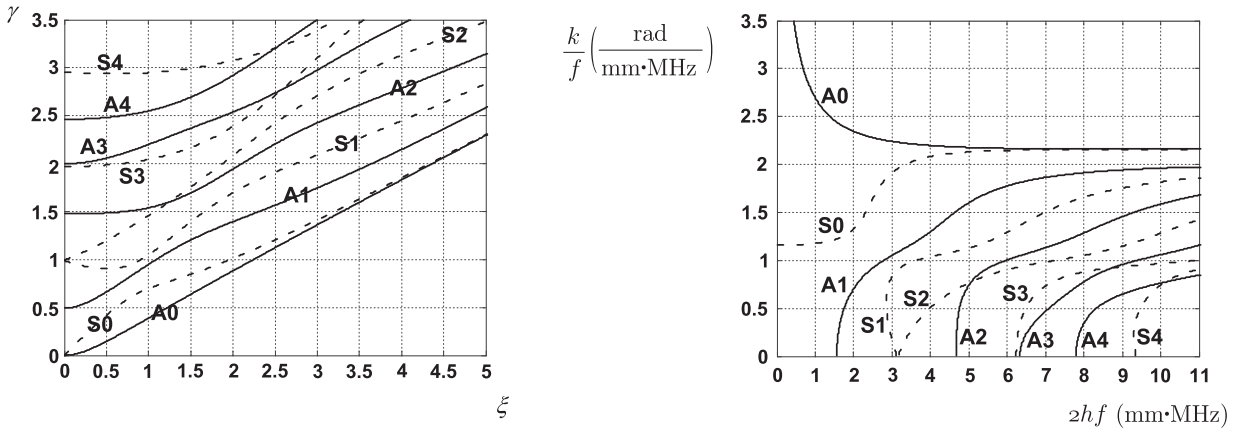

Figure 1. Plots of a) the frequency spectrum and b) of the dispersion curves of the first five antisymmetric (continuous lines) and symmetric (dashed line) Lamb modes for a material with $c_{\mathrm{L}} = 6315$ m/s and $c_{\mathrm{T}} = 3111$ m/s.

its frequency f remains the same, and so do its normalized ξ and regular k wavenumbers. The dispersion curves, which can be derived from the frequency spectrum and are shown in Figure 1b, provide a more straightforward representation of the dependence of the wavenumber k with the plate thickness $2h$ for a given wave frequency f.

2.2 Calculation of the local wavenumber from the out of plane complex displacement fields of surface waves

Given a single-mode monochromatic Lamb wave propagating on a plate, a generic component along the direction of x_i of the displacement vector $\boldsymbol{u}(\boldsymbol{x},t)$ at a point $\mathrm{P} \equiv \boldsymbol{x} = (x_1, x_2)$ of the surface can be described as

$$u_i(\boldsymbol{x},t) = u_{i\mathrm{m}}(\boldsymbol{x},t)\cos\varphi_i(\boldsymbol{x},t) \tag{6a}$$
$$= \mathrm{Re}[\hat{u}_i(\boldsymbol{x},t)] = \mathrm{Re}\{u_{i\mathrm{m}}(\boldsymbol{x},t)\exp[j\varphi_i(\boldsymbol{x},t)]\} \tag{6b}$$
$$= \mathrm{Re}(u_{i\mathrm{m}}[\boldsymbol{x},t]\exp\{j[\varphi_{\mathrm{k}}(\boldsymbol{x}) - 2\pi f t + \varphi_{i0}]\}) \tag{6c}$$

where

$\hat{u}_i(\boldsymbol{x},t)$ is the complex representation,
$u_{i\mathrm{m}}(\boldsymbol{x},t)$ is the local amplitude,
$\varphi_i(\boldsymbol{x},t)$ is the instant local phase, and
φ_{i0} is the initial phase

of the $i-$th component of the displacement vector, and

$$\varphi_{\mathrm{k}}(\boldsymbol{x}) = \int_O^P \boldsymbol{k}(\boldsymbol{x})\cdot d\boldsymbol{x} \tag{7}$$

is the propagation phase-delay of the Lamb wave from a reference wavefront O to the point under consideration P.

If a two dimensional map of the local phase $\varphi_i(\boldsymbol{x},t)$ of any of the components of the displacement vector is measured, by any means, at a given instant t_0, the local wave vector can be calculated as the gradient of such phase

$$\boldsymbol{k}(\boldsymbol{x}) = [k_1(\boldsymbol{x}), k_2(\boldsymbol{x})] = \nabla\varphi_{\mathrm{k}}(\boldsymbol{x}) = \nabla\varphi_i(\boldsymbol{x},t_0) \tag{8}$$

Stroboscopic and pulsed TV holography yield maps of selected components of the instant surface displacement. The phase of the surface wave can then be calculated by applying either temporal,[11] spatial[12] or spatio-temporal[13] evaluation methods. In most of these methods the complex representation of the displacement is calculated during the phase evaluation process sometimes explicitly, sometimes implicitly. The gradient of the phase can be calculated directly from this complex representation,[14] thus avoiding the issues related with the application of discrete gradient filters on wrapped phase maps.

The aforementioned technique, originally developed to calculate the gradient of the optical phase, can be particularized for our application by taking into account that the mechanical phase at the measuring instant t_0 can be expressed as

$$\varphi_i(\boldsymbol{x}, t_0) = \arctan \frac{S_\varphi(\boldsymbol{x})}{C_\varphi(\boldsymbol{x})} = \arctan \frac{\sin[\varphi_i(\boldsymbol{x}, t_0)]}{\cos[\varphi_i(\boldsymbol{x}, t_0)]} \tag{9}$$

where $S_\varphi(\boldsymbol{x})$ and $C_\varphi(\boldsymbol{x})$ are calculated from the measured complex instant displacement field as

$$S_\varphi(\boldsymbol{x}) = \frac{\mathrm{Im}[\hat{u}_i(\boldsymbol{x}, t_0)]}{\mathrm{mod}[\hat{u}_i(\boldsymbol{x}, t_0)]} \tag{10a}$$

$$C_\varphi(\boldsymbol{x}) = \frac{\mathrm{Re}[\hat{u}_i(\boldsymbol{x}, t_0)]}{\mathrm{mod}[\hat{u}_i(\boldsymbol{x}, t_0)]} \tag{10b}$$

the $j-$th component of the wavenumber is then calculated from the fields $S_\varphi(\boldsymbol{x})$ and $C_\varphi(\boldsymbol{x})$ without explicitly calculating the phase by using the following property of the derivative of the arc tangent function

$$k_j(\boldsymbol{x}) = \frac{\partial \varphi_i(\boldsymbol{x}, t_0)}{\partial x_j} = \frac{\partial}{\partial x_j}\left[\arctan \frac{S_\varphi(\boldsymbol{x})}{C_\varphi(\boldsymbol{x})}\right] = C_\varphi(\boldsymbol{x})\frac{\partial S_\varphi(\boldsymbol{x})}{\partial x_j} - S_\varphi(\boldsymbol{x})\frac{\partial C_\varphi(\boldsymbol{x})}{\partial x_j} \tag{11}$$

where the derivatives of $S_\varphi(\boldsymbol{x})$ and $C_\varphi(\boldsymbol{x})$ are approximated by finite difference quotients.

3. MATERIALS AND METHODS

3.1 Test sample

We have tested the proposed method on a $2h = 5,00$ mm thick aluminium plate. The transversal dimensions of the plate (200 mm $\times$ 500 mm) are large enough to prevent the interaction of the Lamb wave with its edges for the width of the wavefronts (see 3.2) and the propagation times (see 3.3) that we use in our experiments. Therefore, this plate can be regarded as infinitely extended in practice.

We have measured the elastic characteristics of this plate by analysing the the propagation of Lamb waves with different frequencies,[15] resulting that the velocities of the longitudinal and shear waves are $c_\mathrm{L} = 6315$ m/s and $c_\mathrm{T} = 3111$ m/s, respectively. This yields the frequency spectrum and dispersion curves shown in Figure 1.

A $0,33$ mm deep X-shaped recess has been machined on the back surface of the plate to simulate a hidden flaw and check for the ability of our technique to detect it. Figure 2 shows a photograph of the recess and how it is placed with respect to the wave generation and measurement systems.

3.2 Wave generation system

We excite Lamb waves in the plate by the widely used prismatic coupling block method.[16] A wedge-shaped block transmits the longitudinal waves generated with a piezoelectric transducer towards the surface of the plate. To get the optimum coupling condition for a given propagation mode, operating frequency f and regular plate thickness $2h$, the incidence angle (also known as wedge angle θ_W, see Figure 2b) must be

$$\theta_\mathrm{W} = \arcsin \frac{c_\mathrm{W}}{c_\mathrm{P}} = \arcsin\left(\frac{c_\mathrm{W}}{2\pi} \cdot \frac{k}{f}\right) \tag{12}$$

where c_W is the longitudinal wave velocity in the wedge and c_P is phase velocity of the selected Lamb mode in the plate. The value of k/f can be read in the ordinate axis of the dispersion curves in Figure 1b.

The plastic wedges used in our experiments have been machined on PMMA ($c_\mathrm{W} = 2,7$ mm/μs) and have a width of 40 mm.

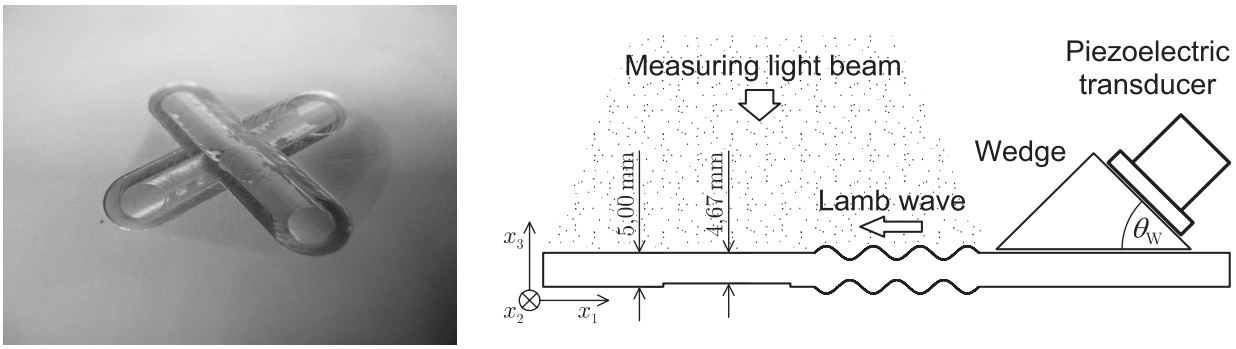

a) b)

Figure 2. (a) Photograph of the test plate showing the X-shaped recess. (b) Orientation of the test plate respect to the wave generation and measuring systems.

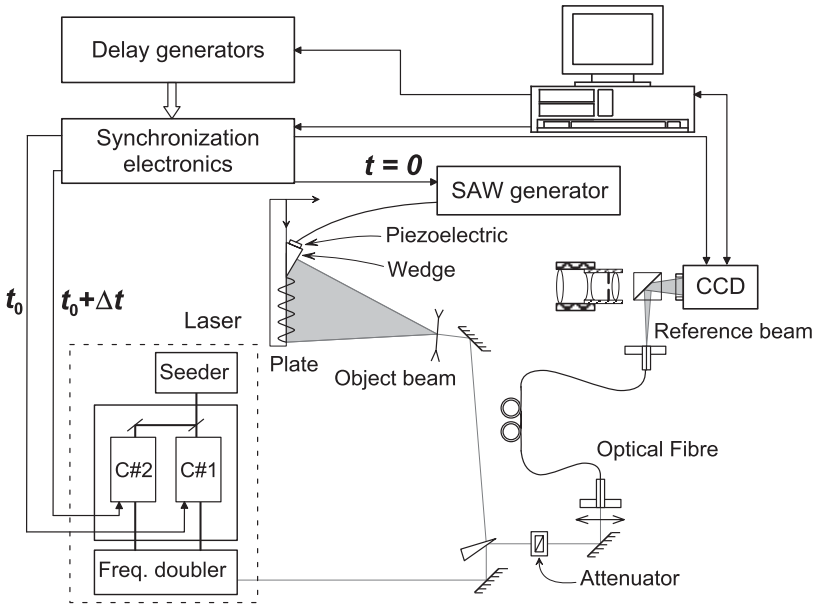

Figure 3. Layout of the TV holography system

3.3 Wave measurement system

A self-developed double-pulsed TV holography system allows us to measure the instant displacement of travelling and standing waves, travelling Lamb waves for this particular application. A twin-cavity pulsed, injection seeded and frequency doubled Nd:YAG laser (Spectron SL404T) is the core of the system. The twin-cavity can produce pairs of pulses with virtually any separation. The pulse duration is approximately 20 ns, which can "freeze" the image of vibrating objects with frequencies up to 50 MHz. As shown in Figure 3 the laser beam is split into an object beam which is expanded to illuminate the object and a reference beam which is directed to the sensor of a CCD camera with the aid of an optical fibre. The object beam is imaged on the CCD where it interferes with the reference beam. The resulting interferogram is spatially sampled with sampling intervals Δx_1 and Δx_2 in such a way that the pixel (m, n) corresponds to the position $\boldsymbol{x}_\mathrm{s} = (m\Delta x_1, n\Delta x_2)$ on the surface of the object. The illumination and observation directions are arranged normal to the surface of the plate to get sensitivity to the out-of-plane component of the displacement $u_3(\boldsymbol{x}, t)$.

The CCD camera (PCO Sensicam Double-Shutter) is able to record pairs of interferograms with a minimum separation of 1 μs. The minimum delay between successive pairs is about 120 ms for the image size (1280×1024 pixel^2) that we have used for our experiments. The synchronizing electronics delays the first laser pulse of each pair from the wave excitation instant by a time t_0 of the order of several tens of microseconds, sufficient

for the wave to cover the whole field of view but short enough to prevent it from reaching the edges of the plate and produce reflected waves which would otherwise interfere with the measurement. The second pulse of each pair is delayed by an small number of half periods of the Lamb wave —just large enough to let the camera record the interferogram corresponding to each pulse in a different image frame— with respect to the first pulse to illuminate the surface in opposite states of vibration and thus obtain the maximum sensitivity to its displacement and maximize the signal to noise ratio.

To measure the displacement of the surface minimizing the errors that the differences between the beams of the two cavities of the laser introduce, we record two pairs of interferograms in fast succession: the first with the Lamb wave travelling the plate and the second without exciting any wave. A 1024×1024 pixel^2 region is selected for processing to facilitate the calculation of the fast Fourier transform. Then we apply a variant[17] of the Fourier transform method which subtracts the artifacts due to the beam mismatch and yields a map of the change of the optical phase $\Delta\Phi(m,n)$ between laser pulses from which the instant out of plane displacement of the surface (Figure 4a) is calculated as

$$u_3(\boldsymbol{x}_\mathrm{s}, t_0) = u_3(m,n) = u_{3\mathrm{m}}(m,n)\cos\varphi_i(m,n) = \frac{\lambda}{8\pi}\Delta\Phi(m,n) \tag{13}$$

with $\lambda = 532$ nm the wavelength of the laser.

The Fourier transform method is then applied to the displacement map,[12] using the periodicity of the wave as a spatial carrier, to get the complex representation of the wave field $\hat{u}_3(m,n)$ (Figure 4b).

3.4 Calculation of the wavevector

The wavevector field $\boldsymbol{k}(m,n)$ is evaluated as the gradient of the mechanical phase, as stated in Equation 8, by calculating its components according to Equation 11.

The amplitude of the wave

$$u_{3\mathrm{m}}(m,n) = \mathrm{mod}[\hat{u}_3(m,n)] \tag{14}$$

shall be calculated to obtain the values of $S_\varphi(m,n)$ and $C_\varphi(m,n)$ by applying Equations 10a and 10b, respectively. It is not necessary to calculate the mechanical phase $\varphi_i(m,n)$.

To approximate the derivatives of $S_\varphi(\boldsymbol{x})$ and $C_\varphi(\boldsymbol{x})$ we use a 2×2 version of the Prewitt operator[18,19]

$$\frac{\partial Q_\varphi}{\partial x_1}(m,n) \approx \frac{\Delta_{x1} Q_\varphi(m,n)}{\Delta x_1} = \frac{1}{\Delta x_1}\frac{Q_\varphi(m+1,n+1) + Q_\varphi(m+1,n) - Q_\varphi(m,n+1) - Q_\varphi(m,n)}{2} \tag{15a}$$

$$\frac{\partial Q_\varphi}{\partial x_2}(m,n) \approx \frac{\Delta_{x2} Q_\varphi(m,n)}{\Delta x_2} = \frac{1}{\Delta x_2}\frac{Q_\varphi(m+1,n+1) + Q_\varphi(m,n+1) - Q_\varphi(m+1,n) - Q_\varphi(m,n)}{2} \tag{15b}$$

where Q_φ stands for either S_φ or C_φ, and $\Delta_{xi} Q_\varphi$ is the finite difference of Q_φ in the direction of x_i. Though the resulting value is stored in the pixel (m,n), it should be assigned to a virtual pixel $\left(m+\frac{1}{2}, n+\frac{1}{2}\right)$ corresponding to the position $\left(x_1 + \frac{1}{2}\Delta x_1, x_2 + \frac{1}{2}\Delta x_2\right) = \boldsymbol{x}_\mathrm{s} + \frac{1}{2}\Delta\boldsymbol{x}$.

We take as values for $C_\varphi\left(\boldsymbol{x}_\mathrm{s} + \frac{1}{2}\Delta\boldsymbol{x}\right)$ and $S_\varphi\left(\boldsymbol{x}_\mathrm{s} + \frac{1}{2}\Delta\boldsymbol{x}\right)$ the averages of their respective values in the four pixels involved in the calculation of the finite differences

$$\bar{Q}_\varphi(m,n) = \frac{1}{4}[Q_\varphi(m,n) + Q_\varphi(m+1,n) + Q_\varphi(m,n+1) + Q_\varphi(m+1,n+1)] \tag{16}$$

and finally obtain the components of the wavevector (Figure 4c) as

$$k_i(m,n) = \bar{C}_\varphi(m,n)\frac{\Delta_{xi} S_\varphi(m,n)}{\Delta x_i} - \bar{S}_\varphi(m,n)\frac{\Delta_{xi} C_\varphi(m,n)}{\Delta x_i} \quad ; \quad i \in \{1,2\} \tag{17}$$

from which the wavenumber,

$$k(m,n) = |\boldsymbol{k}(m,n)| = \sqrt{k_1^2(m,n) + k_2^2(m,n)} \tag{18}$$

a)

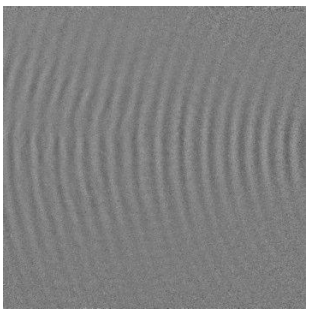

$u_3(\boldsymbol{x}_\mathrm{s}, t_0)$

b)

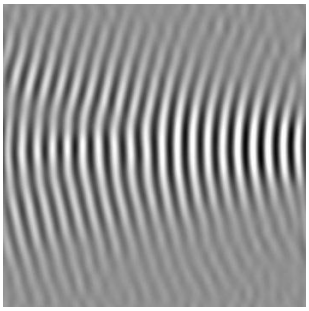

$\mathrm{Re}[\hat{u}_3(\boldsymbol{x}_\mathrm{s}, t_0)]$

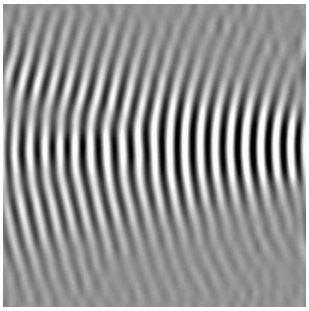

$\mathrm{Im}[\hat{u}_3(\boldsymbol{x}_\mathrm{s}, t_0)]$

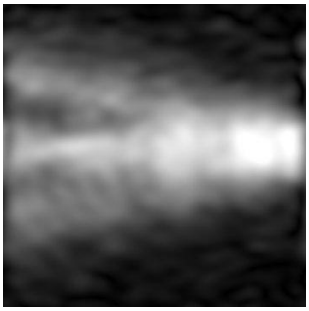

$u_{3,\mathrm{m}}(\boldsymbol{x}_\mathrm{s}) = \mathrm{mod}[\hat{u}_3(\boldsymbol{x}_s, t_0)]$

c)

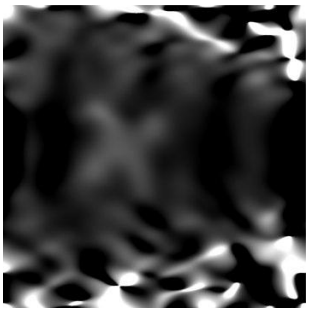

$k_1(\boldsymbol{x}_\mathrm{s}) = \dfrac{\partial \varphi_3(\boldsymbol{x}_\mathrm{s}, t_0)}{\partial x_1}$

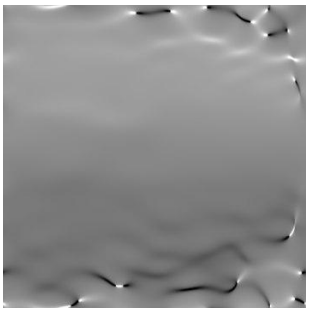

$k_2(\boldsymbol{x}_\mathrm{s}) = \dfrac{\partial \varphi_3(\boldsymbol{x}_\mathrm{s}, t_0)}{\partial x_2}$

d)

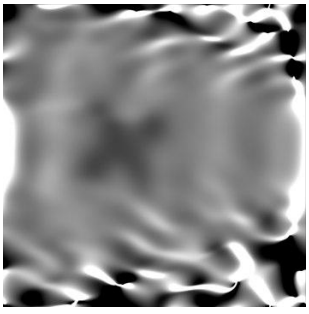

$k(\boldsymbol{x}_\mathrm{s}) = |\boldsymbol{k}(\boldsymbol{x}_\mathrm{s})| = |\nabla \varphi_3(\boldsymbol{x}_\mathrm{s}, t_0)|$

$\theta(\boldsymbol{x}_\mathrm{s}) = \arctan \dfrac{k_2(\boldsymbol{x}_\mathrm{s})}{k_1(\boldsymbol{x}_\mathrm{s})}$

Figure 4. Results of the three stages of the measurement process; a) Optical evaluation with the Fourier transform method (FTM), b) Mechanical evaluation with the FTM, c) and d) Calculation of the wavevector as the gradient of the mechanical phase. Grey level scales are arbitrary; white represents values more positive than black.

and the propagation direction of the wave with respect to the positive direction of the x_1 axis

$$\theta(m,n) = \arctan \frac{k_2(m,n)}{k_1(m,n)} \tag{19}$$

can be calculated as shown in Figure 4d.

The estimated resolution limit of our system for the regular ESPI operation mode[20] —i.e., yielding the difference of two interferograms— is $u_{3\mathrm{m,min}} \approx 0,5$ nm. Therefore, we take the conservative criterion of excluding from the result and set to zero in the maps every pixel where the measured amplitude of the Lamb wave is $u_{3,\mathrm{m}}(m,n) < 1$ nm at any of the four points used to evaluate the wavenumber. Figure 4d shows a raw wavenumber map which corresponds to the one presented in the first row (a) of Figure 5, where the maps have been masked according to this criterion.

4. EXPERIMENTAL RESULTS AND DISCUSSION

Figure 5 shows the results obtained with the proposed method for several Lamb wave modes —namely A1, A2, S1 and S2— on the aforementioned test plate. The wave amplitude and wavenumber maps are presented for comparison.

The measured amplitudes range up to near ten nanometres. The field of view is 121 mm × 121 mm and the sampling interval $\Delta x_1 = \Delta x_2 = 0,118$ mm.

Although the frequencies have not been optimized to provide the maximum sensitivity to thickness changes, all of these four wavenumber maps show clearly the presence, position and shape of the flaw.

Modes A2, S1 and S2 (Figures 5b, 5c and 5d, respectively) are more directional than A1 (Figure 5a) and, consequently, they cover a smaller region of the plate. This capability to cover a larger area of inspection can be a decision criterion to choose among several modes with similar sensitivity to thickness changes.

The amplitude of modes A1 and S2 (Figures 5a and 5d) show some signs of diffraction which could indicate the presence of the flaw and roughly its position, but give no information regarding its shape. There are no traces of amplitude perturbation in modes A2 and S1 (Figures 5b and 5c). In any case, the wavenumber map has proven to be superior in revealing the flaw.

5. CONCLUSIONS

The proposed technique, consisting in mapping the local wavenumber of narrowband Lamb waves as the modulus of the gradient of the mechanical phase measured by pulsed TV holography, has proven to be well suited to detect small thickness inhomogeneities in thin plates.

It is not only capable of revealing the presence of flaws but of visualizing their positions and shapes as well. In this sense, wavenumber maps are superior to wave amplitude maps at least for small thickness changes.

A proper choice of the Lamb mode and frequency is necessary to either maximize one, maybe both, or get a balance between the sensitivity to the changes of thickness and the area covered by the probing wave.

The implementation of this method is simpler and requires less computational effort than numerically solving the inverse scattering problem but, contrary to the latter, its applicability range is limited to small thickness changes which do not produce significant attenuation of the amplitude of the probing wave.

Future development of this technique could lead to permit the characterization of the thickness of the flaw too.

ACKNOWLEDGMENTS

This work was co-funded by the Spanish *Ministerio de Educación y Ciencia* and by the European Commission (ERDF) in the context of the *Plan Nacional de I+D+i* (project number DPI2005-09203-C03-01) and by the *Dirección Xeral de Investigación, Desenvolvemento e Innovación da Xunta de Galicia* in the context of the *Plan Galego de IDIT* (project number PGIDIT06PXIC303193PN). Supplementary co-funding from the *Universidade de Vigo* (project number I608122F64102) is also acknowledged. Machining of ultrasound generating hardware, special optomechanic elements and samples was made by the technician Mr. Pablo Barreiro.

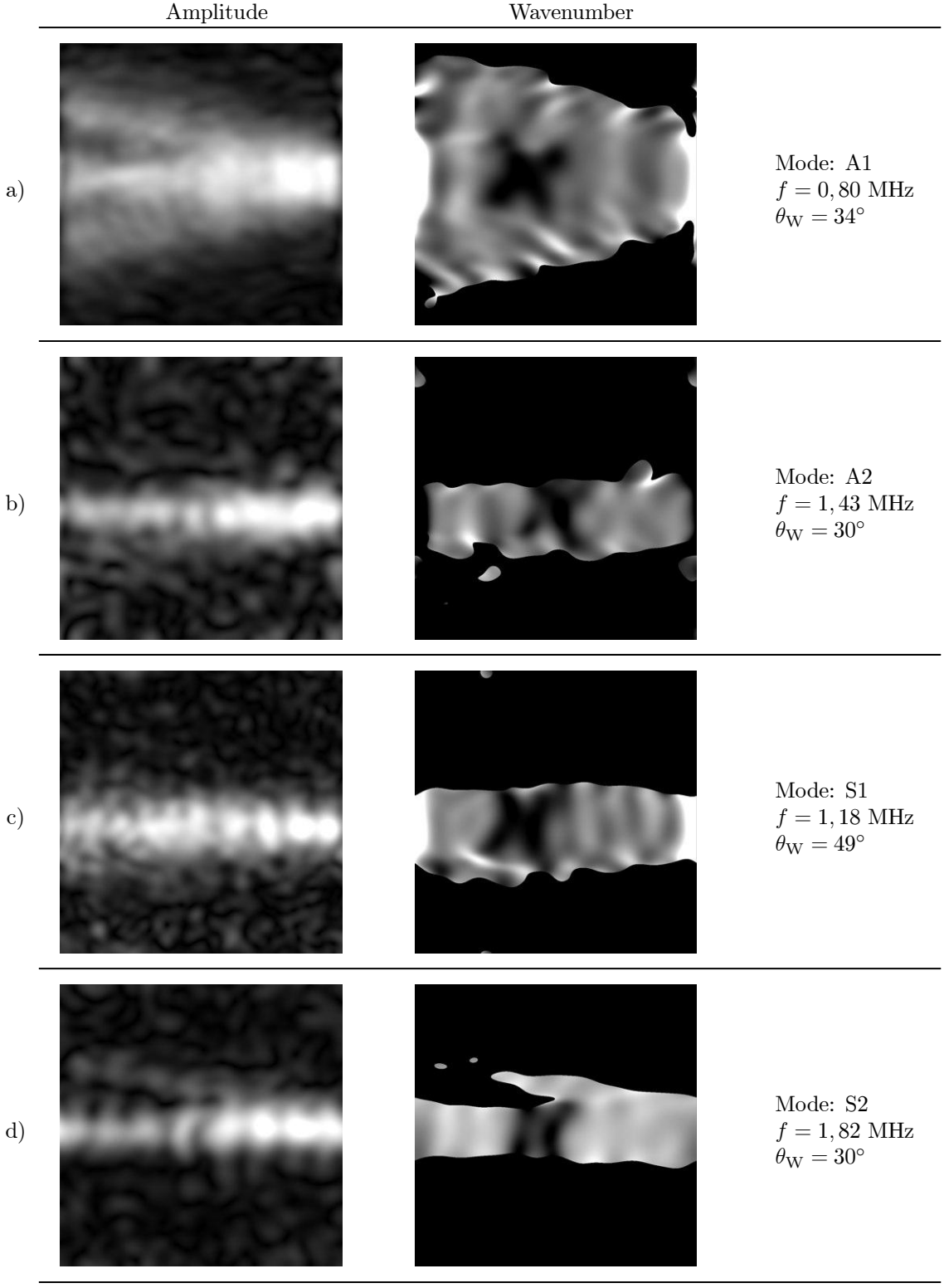

Figure 5. Measurements of the amplitude and wavenumber of four Lamb wave modes propagating from right to left on a test plate with a simulated flaw. The field of view is $121\,\mathrm{mm} \times 121\,\mathrm{mm}$; the modes, frequencies f and wedge angles θ_W as indicated.

REFERENCES

[1] Chimenti, D. E., "Guided waves in plates and their use in materials characterization," *Applied Mechanics Reviews* **50**(5), 247–284 (1997).

[2] Alleyne, D. N. and Cawley, P., "The interaction of Lamb waves with defects," *IEEE Transactions on Ultrasonics, Ferroelectrics and Frequency Control* **39**(3), 381–397 (1992).

[3] Lowe, M. J. S. and Diligent, O., "Low-frequency reflection characteristics of the s0 Lamb wave from a rectangular notch in a plate," *Journal of the Acoustical Society of America* **111**(1), 64–74 (2002).

[4] Fromme, P. and Sayir, M. B., "Measurement of the scattering of a Lamb wave by a through hole in a plate," *Journal of the Acoustical Society of America* **111**(3), 1165–1170 (2002).

[5] Dewhurst, R. J., Edwards, C., McKie, A. D. W., and Palmer, S. B., "Estimation of the thickness of thin metal sheet using laser generated ultrasound," *Applied Physics Letters* **51**(14), 1066–1068 (1987).

[6] Jenot, F., Ouaftouh, M., Duquennoy, M., and Ourak, M., "Corrosion thickness gauging in plates using Lamb wave group velocity measurements," *Measurement Science & Technology* **12**(8), 1287–1293 (2001).

[7] Pei, J., Yousuf, M. I., Degertekin, F. L., Honein, B. V., and Khuri-Yakub, B. T., "Lamb wave tomography and its application in pipe erosion/corrosion monitoring," *Research in Nondestructive Evaluation* **8**(4), 189–197 (1996).

[8] Fernández, J. L., Doval, A. F., Trillo, C., Deán, J. L., and López, J. C., "Video ultrasonics by pulsed TV holography: A new capability for non-destructive testing of shell structures," *International Journal of Optomechatronics* **1**(2), 122–153 (2007).

[9] Mast, T. D. and Gordon, G. A., "Quantitative flaw reconstruction from ultrasonic surface wavefields measured by electronic speckle pattern interferometry," *IEEE Transactions on Ultrasonics, Ferroelectrics, and Frequency Control* **48**(2), 432–444 (2001).

[10] Graff, K. F., [*Wave motion in elastic solids*], Dover, New York (1975).

[11] Valera, J. D., Doval, A. F., and Jones, J. D. C., "Determination of vibration phase with electronic speckle pattern interferometry (ESPI)," *Electronics Letters* **28**(25), 2292–2294 (1992).

[12] Trillo, C., Doval, A. F., Cernadas, D., López, O., López, J. C., Dorrío, B. V., Fernández, J. L., and Pérez-Amor, M., "Measurement of the complex amplitude of transient surface acoustic waves using double-pulsed TV holography and a two-stage spatial Fourier transform method," *Measurement Science & Technology* **14**(12), 2127–2134 (2003).

[13] Trillo, C. and Doval, A. F., "Spatiotemporal Fourier transform method for the measurement of narrowband ultrasonic surface acoustic waves with TV holography," in [*Speckle06: Speckles, From Grains to Flowers*], Slangen, P. and Cerruti, C., eds., *Proceedings of SPIE* **6341**, 63410M–1–6 (2006).

[14] Singh, H. and Sirkis, J. S., "Direct extraction of phase gradients from Fourier-transform and phase-step fringe patterns," *Applied Optics* **33**(22), 5061–5020 (1994).

[15] Deán, J. L., Fernández, J. L., Doval, A. F., and Trillo, C., "Measurement of lamb waves dispersion curves under narrowband monomode excitation using tv holography," in [*Speckle06: Speckles, From Grains to Flowers*], Slangen, P. and Cerruti, C., eds., *Proceedings of SPIE* **6341**, 63410B–1–6 (2006).

[16] Viktorov, I. A., [*Rayleigh and Lamb waves. Physical theory and applications*], Plenum Press, New York (1967).

[17] Trillo, C., Doval, A. F., and Pérez-Amor, M., "Enhanced measurement of ultrasonic surface acoustic waves with TV holography by correction of phase mismatch between laser cavities," in [*Speckle06: Speckles, From Grains to Flowers*], Slangen, P. and Cerruti, C., eds., *Proceedings of SPIE* **6341**, 63412X–1–6 (2006).

[18] Rosenfeld, A. and Kak, A. C., [*Digital picture processing (Second edition)*], vol. 2, Academic Press, San Diego (1981).

[19] Davies, E. R., [*Machine vision: theory, algorithms, practicalities*], Academic Press, London (1990).

[20] Cernadas, D., Trillo, C., Doval, A. F., López, J. C., Dorrío, B. V., Fernández, J. L., and Pérez-Amor, M., "Non-destructive testing with surface acoustic waves using double-pulse TV holography," *Measurement Science & Technology* **13**(4), 438–444 (2002).